Energy-dependent relaxation time in quaternary amorphous oxide semiconductors probed by gated Hall effect measurements

Josephine Socratous,[1] Shun Watanabe,[1,2,3] Kulbinder K. Banger,[1] Christopher N. Warwick,[1] Rita Branquinho,[4] Pedro Barquinha,[4] Rodrigo Martins,[4] Elvira Fortunato,[4] and Henning Sirringhaus[1,*]

[1]*Cavendish Laboratory, University of Cambridge, J. J. Thomson Avenue, Cambridge CB3 0HE, United Kingdom*

[2]*Department of Advanced Materials Science, Graduate School of Frontier Sciences, The University of Tokyo, 5-1-5 Kashiwanoha, Kashiwa 277-8561, Chiba, Japan*

[3]*JST, PRESTO, 4-1-8 Honcho, Kawaguchi, Saitama 332-0012, Japan*

[4]*i3N/CENIMAT, Department of Materials Science, Faculty of Science and Technology, Universidade NOVA de Lisboa and CEMOP/UNINOVA, Campus de Caparica, 2829-516 Caparica, Portugal*

(Received 2 March 2016; revised manuscript received 19 September 2016; published 18 January 2017)

Despite the success of exploiting the properties of amorphous oxide semiconductors for device applications, the charge transport in these materials is still not clearly understood. The observation of a definite Hall voltage suggests that electron transport in the conduction band is free-electron-like. However, the temperature dependence of the Hall and field-effect mobilities cannot be explained using a simple bandlike model. Here, we perform gated Hall effect measurements in field-effect transistors, which allow us to make two independent estimates of the charge carrier concentration and determine the Hall factor providing information on the energy dependence of the relaxation time. We demonstrate that the Hall factor in a range of sputtered and solution-processed quaternary amorphous oxides, such as a-InGaZnO, is close to two, while in ternary oxides, such as InZnO, it is near unity. This suggests that quaternary elements like Ga act as strong ionized impurity scattering centers in these materials.

DOI: 10.1103/PhysRevB.95.045208

Amorphous oxide semiconductors (AOSs) have recently been widely investigated for thin-film transistor (TFT) applications due to their high mobilities exceeding values of 1–10 $cm^2\ V^{-1}\ s^{-1}$ and improved stability compared to silicon devices. Most devices are deposited via sputtering methods but there have also been recent approaches to produce similar performance levels by low-temperature solution processing approaches [1–3]. Despite the rapid commercialization of AOS technology in display applications, a charge transport model that explains all the experimental observations is still missing. In 2004, Nomura *et al.* reported the first amorphous metal oxide as the semiconducting layer in a TFT [4]. Measurements of the Hall effect have contributed much to the understanding of the transport properties of AOSs. In contrast to a-Si, the Hall effect displays the sign of electron transport without sign anomaly. Hall measurements have typically been interpreted by assuming that the Hall effect is ideal, i.e., that the Hall resistance is the inverse of the carrier concentration times the electron charge. However, the Hall mobility was found to be carrier concentration dependent and thermally activated [5], both observations contradicting a simple free-electron bandlike transport model and potentially suggesting a hopping mechanism. The latter is, however, incompatible with an ideal Hall effect theory because this is generally understood within semiclassical Boltzmann transport theory with a relaxation time approximation, a parameter that has no physical meaning in a hopping conduction model. Arrhenius-type thermally activated behavior is also observed in a-Si:H but in that case the Hall effect is anomalous and both observations are consistent with a variable range hopping (VRH) model [6–8]. Recently, Germs *et al.* [9] attempted to describe transport in AOSs by including VRH behavior below a mobility edge. Although this model resulted in decent fits of the field-effect mobility, it required that 99% of the transport originates from hopping. This result contradicts the high carrier mobility and the well-defined Hall effect in amorphous oxides. In an attempt to unify the contradicting experimental observations, Kamiya *et al.* [10] proposed a transport model based on percolation theory. Such a model was previously proven to lead to temperature dependencies similar to those observed in hopping regimes [11]. While the percolation conduction model was found to explain well the behavior of the Hall mobility [10,12], the peculiar behavior of the field-effect mobility which also shows activationlike behavior still remains to be treated. Lee *et al.* [13] used a combined trap limited and percolation conduction model to describe the field-effect mobility. They concluded that transport is dominated by traps when the density of tail states below the conduction band edge is larger than $10^{20}\ eV^{-1}\ cm^{-3}$, otherwise percolation conduction is dominant. While this model explained the gate dependence of the field-effect mobility at room temperature, it did not take into account its temperature dependence. Abe *et al.* reproduced the current-voltage (I-V) characteristics of a-InGaZnO TFTs using a carrier concentration dependent drift mobility model [14]. This model leads to a power law of the field-effect mobility, similar to the one obtained in an exponential subgap trap model in a-Si:H. However, the predicted temperature dependence of the two models is very different and the a-Si:H model cannot explain the observed temperature dependence in a-InGaZnO TFTs. It is, therefore, likely that the field-effect mobility's behavior is indicative of a density of states-energy landscape above the conduction band rather than below it. Summarizing, the insight gained from several, previous studies points tentatively to an energy (or carrier concentration) dependence of the drift mobility and relaxation time of carriers in the conduction band, but no direct experimental observation of this has yet been made [15,16].

*Corresponding author: hs220@cam.ac.uk

 ©2017 American Physical Society

In this report, we use for the first time a gated Hall bar architecture that allows extracting the Hall factor in AOSs, which is a direct measure of the energy dependence of the relaxation time. Our architecture allows for accurate Hall effect measurements without any errors introduced by geometrical factors as, for example, in the more commonly used Van der Pauw methods. Furthermore, the gated Hall bar architecture is based on a field-effect transistor configuration, in which a controlled carrier concentration can be induced by electrostatic gating. This allows us to measure a Hall voltage on intrinsic, low-conductivity films that are of most interest in TFT devices, i.e., there is no need to dope the films by introducing chemical or stoichiometric defects, such as oxygen vacancies. Equation (1) shows how the Hall factor γ_H can be calculated from the Hall coefficient R_H using the measured Hall voltage ΔV_{Hall}, drain current I_{ds} and free carrier concentration n_o:

$$|R_H(V_g)| = \frac{|\Delta V_{Hall}(V_g)|}{I_{ds}(V_g)B} = \frac{1}{en_o}\frac{\langle\tau^2\rangle}{\langle\tau\rangle^2} = \frac{1}{en_o}\gamma_H, \quad (1)$$

where B is the magnetic field, $\langle\tau\rangle$ the average of the energy dependent relaxation time $\langle\tau\rangle = \frac{\int_0^\infty \tau(\epsilon)\epsilon^{\frac{3}{2}}\exp(-\frac{\epsilon}{k_B T})d\epsilon}{\int_0^\infty \epsilon^{\frac{3}{2}}\exp(-\frac{\epsilon}{k_B T})d\epsilon}$, where k_B is the Boltzmann constant [17]. In ordinary, nongated Hall effect measurements on a suitably doped, conducting film, n_o is not known; in fact the usual assumption when interpreting such measurements is that γ_H is unity, which is then used to determine the free carrier concentration per unit volume. In the case of Hall effect measurements on field-effect transistor (FET) structures, the above 3D equation is converted to a 2D form and n_o denotes the carrier concentration per unit area, as our Hall measurements are performed on FET devices where the channel layer is assumed to form within a very thin layer of the interface between the semiconductor and the dielectric. In this paper, n_o will denote carrier concentration per unit area and can be determined independently from the product of the measured gate dielectric capacitance and the applied voltage, allowing a direct, experimental determination of γ_H. The Hall factor can also be calculated from the ratio of the Hall μ_H to the four-point-probe field-effect mobility μ_{4pp} [Eq. (2)]:

$$\mu_H(V_g) = |R_H(V_g)|\sigma_{4pp}(V_g) = \gamma_H\mu_{4pp}(V_g), \quad (2)$$

where σ_{4pp} is the four-point-probe conductivity. Interestingly, we find that γ_H in both sputtered and solution-processed a-InGaZnO and other InZnO-based quaternary systems is near twice the ideal value. A nonunity value of the Hall factor suggests an energy dependent relaxation for which $\langle\tau^2\rangle \neq \langle\tau\rangle^2$.

Our gated Hall bar measurements use a bottom-gate, top-contact configuration on Si/SiO_2 shown in Fig. 1(a). After deposition, the semiconductor is removed from all the unwanted regions around the contacts allowing for the formation of a well-defined channel. A detailed description of the fabrication process can be found in Sec. A of Ref. [18]. Our Hall bars had very small gate leakage, negligible contact resistance (~0.2% of the channel resistance), and a very small transverse voltage difference at zero magnetic field. These allow for very accurate measurements with minimal errors. Figures 1(b) and 1(c) show typical transfer and output characteristics measured on our Hall bars with a solution-processed InGaZnO semiconducting layer. The solution was prepared from commercially available nitrate-based precursors which were mixed in a molar ratio of In:Zn:Ga = 57:38:5. The device exhibits good TFT characteristics with a mobility close to 2 $cm^2 V^{-1} s^{-1}$, small hysteresis and sufficiently large on-off ratios ($>10^5$).

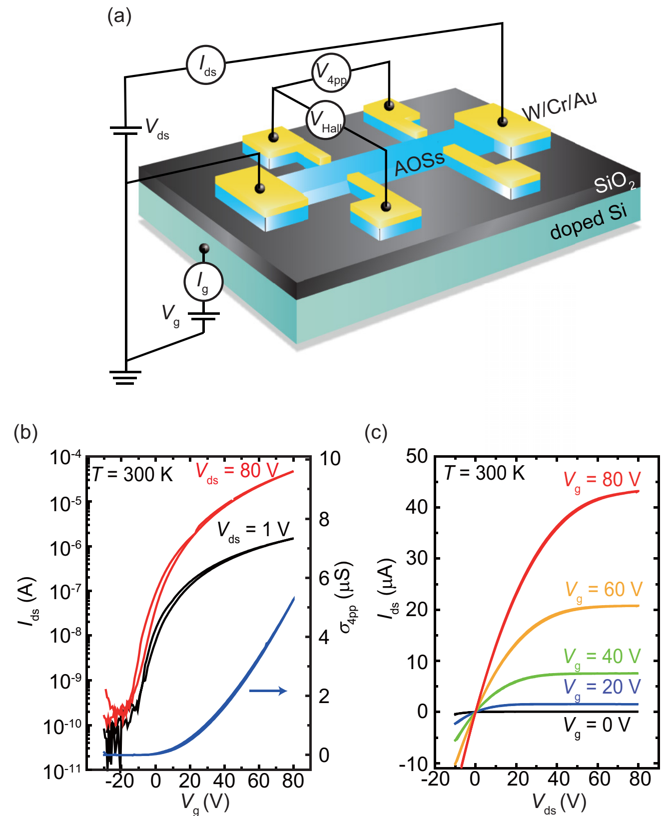

FIG. 1. Concept of gated Hall effect measurements. (a) Schematic illustration of a gated Hall bar structure, where the metal oxide semiconductor layers were deposited either by spin-coating from a solution or sputtering. A hybrid metal contact, W (40 nm)/Cr (1.5 nm)/Au (60 nm) was then deposited directly on the top of the semiconducting layer. Here, I_{ds}, I_g, V_{ds}, V_g, V_{4pp}, and V_{Hall} denote the source-drain current, gate leakage current, source-drain voltage, gate voltage, four-point probe voltage, and Hall voltage, respectively. (b) Typical transfer and (c) output TFT characteristics measured in the gated Hall bar structure with the solution-processed a-InGaZnO. Hysteresis is clockwise. The V_g dependence of the four-point probed transconductance, σ_{4pp}, is also shown.

Figure 2(a) shows the evolution of the Hall voltage ΔV_{Hall} while sweeping the magnetic field of the a-InGaZnO device shown in Fig. 1(a) for different gate voltages at room temperature. From these data, we can calculate the Hall coefficient R_H and Hall mobility μ_H, using Eqs. (1) and (2) (see Sec. B in Ref. [18] for measurement details). The Hall voltage increases proportional to the magnetic field and its sign represents n-type transport as expected for a-InGaZnO. In Fig. 2(b), we compare the inverse Hall coefficient to the gate-induced, free carrier concentration obtained from the measured capacitance of the gate dielectric (black line). The detailed capacitance measurements are shown in Sec. C

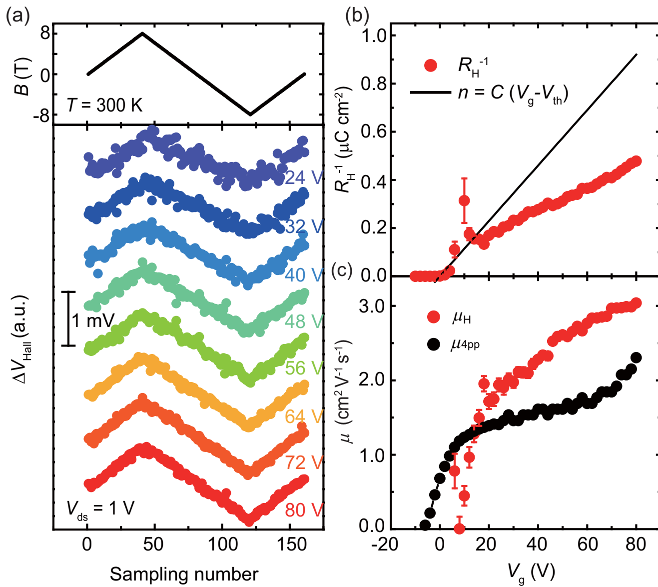

FIG. 2. Gated Hall effect measurements in solution-processed a-InGaZnO. (a) The applied magnetic field B (top) and Hall signals V_{Hall} (bottom) measured for the solution-processed a-InGaZnO are plotted. To ensure the transistors are in the linear regime the measurements were performed with applying small $V_{\mathrm{ds}} = 1.0V$. Details can be found in Sec. B in Ref. [18]. (b) V_{g} dependence of inverse Hall coefficient, R_{H}^{-1}, measured for the solution-processed a-InGaZnO. The solid line represents the charge concentration estimated from the capacitance, $n = C(V_{\mathrm{g}} - V_{\mathrm{th}})$ where V_{th} denotes the threshold voltage. (c) V_{g} dependence of Hall μ_{H} (red) and four-point-probe field-effect $\mu_{4\mathrm{pp}}$ (black) mobilities.

in Ref. [18]. Assuming that the vast majority of charges induced by the gate voltage is indeed free, the ratio between the slopes of the two curves gives the value of the Hall factor γ_{H} [Eq. (1)]. Alternatively, the Hall factor can also be estimated from the ratio of the Hall and the contact-resistance corrected, four-point-probe mobility [Eq. (2)]. Both mobilities are shown in Fig. 2(c) as a function of gate voltage. Interestingly, from both methods, we observe that the Hall factor is not close to the ideal value ($\gamma_{\mathrm{H}} \sim 1$) but exceeds this value by a factor of two. For determining the Hall factor, we have found the extraction from the Hall resistance more accurate than from the Hall mobility. This is because the extraction of the four-point probe mobility involves taking a derivative of the measured current as a function of gate voltage and this makes its extraction prone to artifacts. For example, the four-point probe mobility in nitrate IGZO exhibits an increase above 60 V, which we believe is an artefact of the mobility extraction due to parasitic leakage paths in our Hall bar architecture as this was not observed in normal FET structures. In contrast, the extraction of the Hall mobility and the extraction of the Hall carrier concentration do not involve taking a derivative and this makes them less prone to artifacts. For this reason, we primarily extract the Hall factor from the Hall resistance at high gate voltages. It should be noted that no clear magnetoresistance is seen in the gated Hall measurements (see Sec. D in Ref. [18]).

We repeated the measurements for a device for which a-InGaZnO was deposited via sputtering. The Hall voltage signal was distinguishable at temperatures as low as 60–80 K (Fig. 3) and we were able to extract the Hall factor up to temperature. The room-temperature Hall factor is close to two, in agreement with the results for the solution-processed device. At lower temperatures, the Hall factor increases rapidly and reaches values of 3–3.5. At the lowest temperatures (60–80 K), the signal-to-noise ratio of the measurements becomes insufficient to determine the temperature dependence accurately.

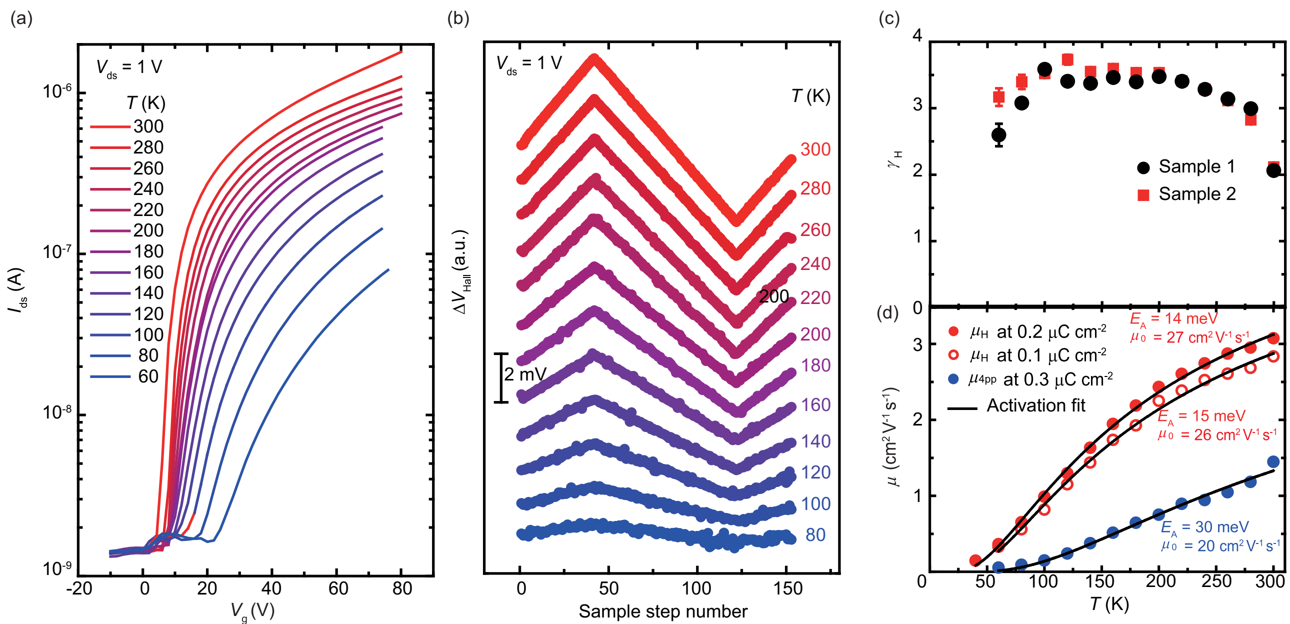

FIG. 3. Temperature-dependent Hall measurements for a sputtered InGaZnO device. (a) Transfer curves, (b) Hall voltage, (c) Hall factor, and (d) Hall and four-point probe field-effect mobility. The results were reproducible for more than one sputtered device. The extracted parameters from the activation fits are different to the solution processed devices due to the different composition of the material and trap states associated with the deposition process.

Before we can interpret the Hall factor in terms of an energy-dependent relaxation time, we need to review the validity of one of the key assumptions made in the discussion so far. We have assumed that all gate-induced charges are mobile and contribute to the Hall voltage. If there was a significant fraction of trapped charges, our measurement would extract an effective Hall factor $\gamma_{\rm H}^{'}$, which is enhanced over the true Hall factor determined by the energy dependence of the relaxation time by a factor $f_{\rm f}^{-1}$, where $f_{\rm f}$ is the ratio of the free to the total number of gate induced charges:

$$\gamma_{\rm H}^{'} = \frac{C(V_{\rm g} - V_{\rm th})}{R_{\rm H}^{-1}} = \frac{en_{\rm o}}{f_{\rm f} R_{\rm H}^{-1}} = \frac{\gamma_{\rm H}}{f_{\rm f}}. \quad (3)$$

In other words, there are in principle two different explanations for a Hall factor of two: the first one is attributed to trapping with $\gamma_{\rm H} = 1$ and $f_{\rm f} = 0.5$, i.e., half of the gate-induced charges are trapped. The second one is attributed to an intrinsic scattering mechanism with $\gamma_{\rm H} = 2$ and $f_{\rm f} = 1$. Figure 3(d) shows that both Hall and four-point-probe mobilities follow activationlike behavior but the latter has a higher activation energy. This discrepancy suggests that, at least partly, the field-effect and Hall mobilities represent the characteristics of different energetic states. The Hall mobility reflects the distribution at and above the conduction band while the field-effect mobility can also reflect the properties of states below the conduction band. The Hall mobility's activation behavior can be explained by the percolation conduction model while the higher activation energy of the four-point-probe mobility is indicative of some trapping at low temperature. However, there are several key findings that suggest that at room temperature our explanation in terms of $\gamma_{\rm H} = 2$ is indeed the correct one.

(1) Solution-processed and sputtered devices exhibit strikingly similar values of $\gamma_{\rm H} \approx 2$ at room temperature in spite of the sputtered samples having approximately five times higher field-effect mobilities. Materials deposited by such different routes should have different trap distribution, the sputtered samples are expected to have a significantly, lower trap concentration than the solution processed ones. If $f_{\rm f}$ was deviating significantly from 1, this would lead to different values of $\gamma_{\rm H}^{'}$ in the two samples.

(2) We have observed a systematic dependence of the Hall factor on the chemical composition of the AOS. Figure 4 shows the gate dependence of the inverse Hall coefficient and mobilities for different InZnO-based quaternary systems doped with strontium (InSrZnO), yttrium (InYZnO), barium (InBaZnO), and lanthanum (InLaZnO) as well as the ternary InZnO (In:Zn = 6:4) and binary In_2O_3. The dominant gate voltage dependence of the carrier concentration is linear as one would expect although there are some deviations from linearity, particularly near the transistor onset/threshold voltage. In this regime, the determination of the Hall resistance and Hall mobility is comparatively inaccurate as the channel is more resistive and systematic errors, arising, for example, due to geometric offsets of the voltage probes used to measure the Hall voltage would have to be taken into account before interpreting the carrier concentration in this regime. This is a well-known issue associated with performing Hall measurements on relatively low mobility systems. In the paper we therefore mainly focus on the high gate voltage regime above 30–40 V where the channel is sufficiently conducting that the Hall resistance can be accurately extracted for all materials investigated. In this regime, the carrier concentration increases approximately linearly with gate voltage. For determining the Hall factor, we have found the extraction from the Hall resistance [top panels in Fig. 4, Eq. (1)] more accurate than from the Hall mobility [bottom panels in Fig. 4, Eq. (2)] for the reasons discussed above. Remarkably, all ternary and binary systems investigated show an ideal Hall effect at room temperature with $\gamma_{\rm H} = 1$, whereas all quaternary systems show a Hall factor close to two. The solution-processed InZnO and In_2O_3 have similar field-effect mobilities to the solution-processed InGaZnO ($\sim$2 $\rm cm^2\,V^{-1}\,s^{-1}$) and should, therefore, show a similar Hall factor if $\gamma_{\rm H}$ depended on $f_{\rm f}$. This result clearly points towards a chemical composition-dependent scattering mechanism as the origin of the nonunity Hall factor, and not a trapping-based mechanism.

(3) We performed device modeling to extract the trap tail width $E_{\rm t}$ by assuming an exponential subgap trap model similar to a-Si:H and to what previous reports have used for a-IGZO [14–16]. We fit the drain current at each temperature using $I_{\rm d}(V_{\rm g}) = \alpha(V_{\rm g} - V_{\rm th})^{\beta}$ with β given by $\beta = \frac{T_\gamma}{T} + \beta_{\rm o}$. Here, T_γ and $\beta_{\rm o}$ are parameters and $T_\gamma = 2E_{\rm t}/k_{\rm B}$. We then plot β versus 1/T and extract E_t. Figure 5(a) shows the measured and fitted transfer curves at different temperatures. The extracted β is shown plotted versus $1/T$ in Fig. 5(b). The extracted T_γ is 142.6 K in agreement with previous references [14–16], which find T_γ in the range between 125 and 189 K. This gave a value of 6 meV for $E_{\rm t}$. We used this value together with a worst case scenario for the density of subgap trap states [14] to estimate the ratio of trapped to total charges (Sec. E in Ref. [18]). Our calculations are consistent with previous device modeling [15] and estimate that only less than 10% of the charges are trapped at room temperature. This is too small to explain our observed Hall factor at room temperature. At lower temperatures, trapping becomes more important and $f_{\rm f}$ is likely to become less than 1. The device modeling predicts that trapping is likely to make a contribution to the observed increase in the Hall factor at lower temperatures, although it is difficult to make quantitative predictions about the expected magnitude of the increase because of the difficulties in extracting a reliable parametrization of the density of states.

A Hall factor of two implies a particular energy dependence of the relaxation time, which is determined by the scattering mechanism. Hall factors have been predicted for various scattering mechanisms [17]. For example, lattice scattering with an energy dependence of $\tau \propto E^{-1/2}$ yields $\gamma_{\rm H} = 1.18$. However, for scattering by ionized impurities, which create potential barriers above the conduction band edge, $\tau \propto E^{3/2}$ is predicted theoretically, which yields $\gamma_{\rm H} = 1.93$, close to what we observe for the quaternary AOSs. For example, assuming an accumulation layer thickness of 1 nm, the carrier concentration determined from the inverse Hall coefficient at a gate voltage of $V_{\rm g} - V_{\rm th} = 40$ V is 10^{19} $\rm cm^{-3}$ for the sputtered device, half of what it is for the nitrate IZO device. Our results therefore show that in quaternary AOS dopants, such as Ga, Sr, Y, Ba, or La, act as ionized impurity scattering centres, while in ternary

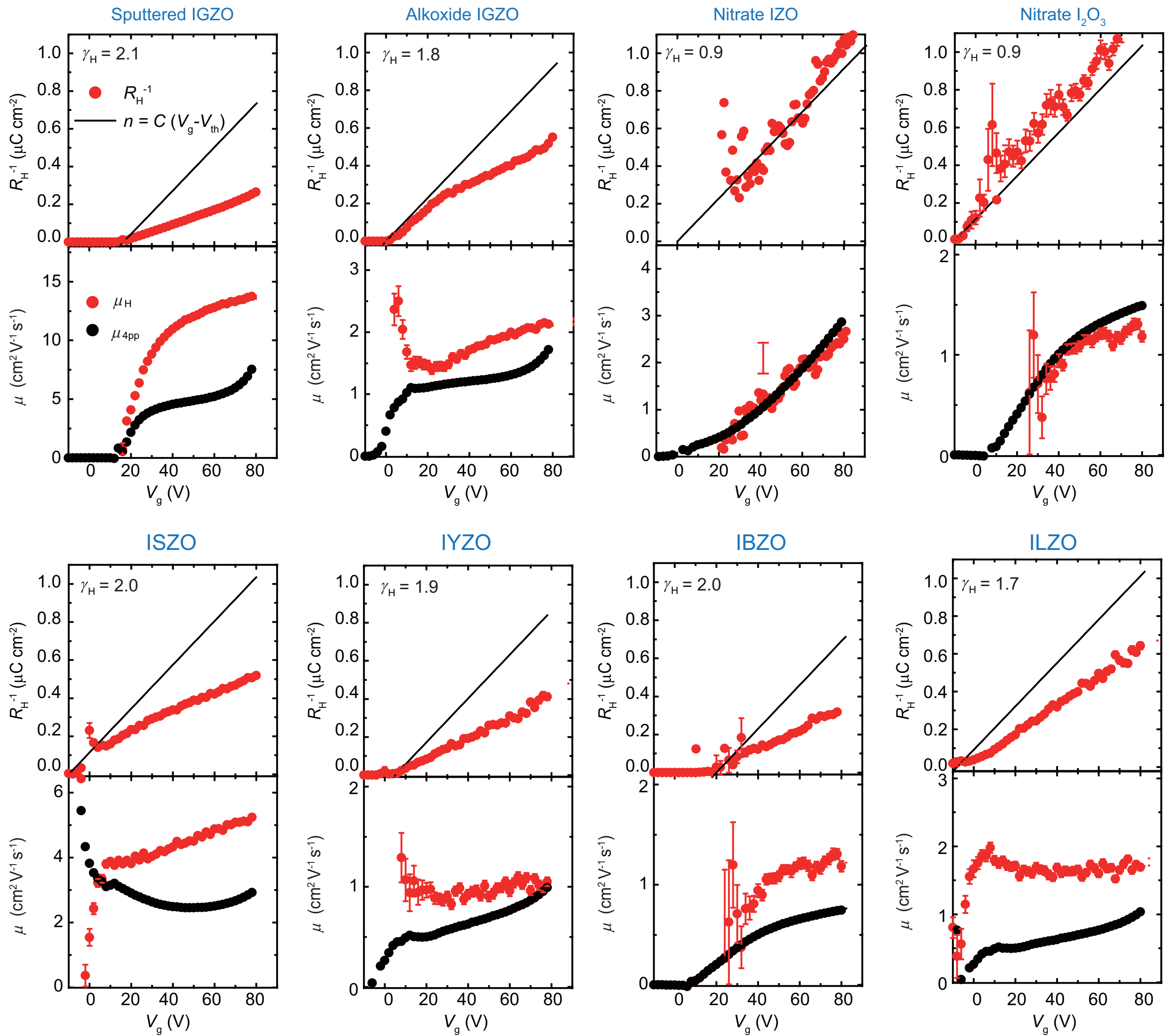

FIG. 4. Gate dependence of inverse Hall coefficient, Hall mobility, and four-point probe field-effect mobility for quaternary, ternary, and binary metal oxide semiconductors. The quaternary systems are InZnO-based and are doped with gallium (InGaZnO), strontium (InSrZnO), yttrium (InYZnO), barium (InBaZnO), and lanthanum (InLaZnO). For the solution-processed quaternary systems in this figure, alkoxide-based precursors have been used.

or binary AOS, such as InZnO and In_2O_3 such scattering mechanisms are not present.

The temperature dependencies of the Hall and field-effect mobilities in Fig. 3(d) are shown to fit well an activation model. The demonstrated temperature dependencies of Hall factor and mobilities may contradict the prediction of the Boltzmann transport framework, i.e., the Hall factor should be independent of temperature and the (drift) mobility should be $\sim T^{\frac{3}{2}}$, unless multiple scattering mechanisms exist. Given the fact that the obtained γ_H shows nonmonotonic temperature behavior, multiple energy-dependent scattering processes can occur with decreasing temperature, which is often seen in nondegenerated semiconductors like Si [19] and Ge [20]. In our case, an increase in the fraction of trapped charges may lead to some modulation of γ_H as the temperature is lowered. More quantitative modeling of the low temperature behavior will be the subject of further work; here we focus on interpreting the room temperature behavior, which we believe to be largely unaffected by trapping.

The results obtained from our gated Hall bar measurements shed new light on the transport physics of AOS. The scattering mechanism in these materials has been intensely debated [9,13,14] but no direct measurements have been available. Our results show unambiguously that in quaternary oxides dopants like Ga are not merely acting as to chemically control the oxygen vacancy concentration [21,22] without affecting carrier transport in the conduction band, as commonly believed. These dopants constitute in fact strong ionized impurity scattering centers for the conduction band electrons that govern their transport properties. Such detailed insight into

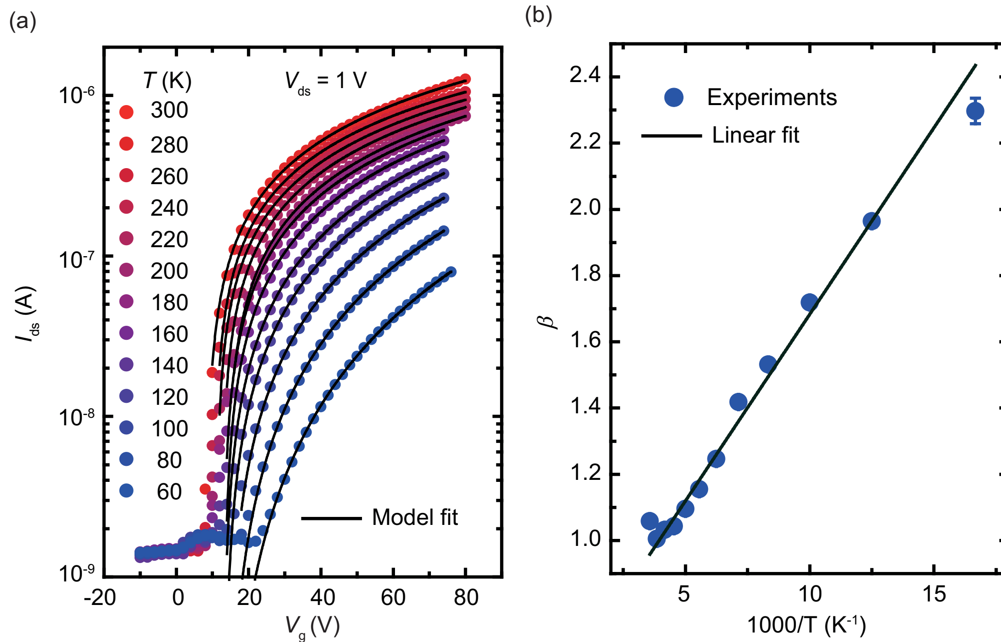

FIG. 5. I-V characteristics at different temperatures obtained from a Hall bar with a sputtered a-IGZO. (a) The transfer curves are fitted with an equation of the form $I_d = \alpha(V_g - V_{th})^{\beta}$. (b) β vs $1/T$

the scattering mechanisms in AOS using novel experimental tools is needed in order to better understand the transport physics of this important class of electronic materials and to develop AOS with further improved device performance.

We acknowledge funding from the European Union Seventh Framework Programme (FP7/2007-2013) under Grant Agreement No. 263042 as well as the Portuguese Science Foundation through the Project UID/CTM/50025/2013. J.S. thanks the Engineering and Physical Sciences Research Council and the A. G. Leventis Foundation for funding. S. W. is supported by Grant-in-Aid for JSPS Fellowship, and thanks PRESTO, JST for funding. The authors declare no competing financial interests.

J.S. and S.W. designed and performed the experiments and analyzed the data. J.S., K.B.B., and S.W. established the etching method and fabricated all the devices. R.B., P.B., and E.F. supplied the sputtered IGZO film. C.N.W. helped with device modeling. J.S., S.W., and H.S. wrote the manuscript and Supplemental Material. S.W. and H.S. supervised all the work. All authors discussed results and reviewed the manuscript.

J.S. and S.W. contributed equally to this work.

[1] K. K. Banger, Y. Yamashita, K. Mori, R. L. Peterson, T. Leedham, J. Rickard, and H. Sirringhaus, Low-temperature, high-performance solution-processed metal oxide thin-film transistors formed by a 'sol-gel on chip' process, Nat. Mater. **10**, 45 (2011).

[2] M.-G. Kim, M. G. Kanatzidis, A. Facchetti, and T. J. Marks, Low-temperature fabrication of high-performance metal oxide thin-film electronics via combustion processing, Nat. Mater. **10**, 382 (2011).

[3] Y. Hwan Hwang, J.-S. Seo, J. Moon Yun, H. Park, S. Yang, S.-H. Ko Park, and B.-S. Bae, An 'aqueous route' for the fabrication of low-temperature-processable oxide flexible transparent thin-film transistors on plastic substrates, NPG Asia Mater. **5**, e45 (2013).

[4] K. Nomura, H. Ohta, A. Takagi, T. Kamiya, M. Hirano, and H. Hosono, Room-temperature fabrication of transparent flexible thin-film transistors using amorphous oxide semiconductors, Nature (London) **432**, 488 (2004).

[5] A. Takagi, K. Nomura, H. Ohta, H. Yanagi, T. Kamiya, M. Hirano, and H. Hosono, Carrier transport and electronic structure in amorphous oxide semiconductor, a-InGaZnO4, Thin Solid Films **486**, 38 (2005).

[6] L. Friedman, Hall conductivity of amorphous semiconductors in the random phase model, J. Non-Cryst. Solids **6**, 329 (1971).

[7] L. Friedman, The Hall effect in ordered and disordered systems, Philos. Mag. B **38**, 467 (1978).

[8] D. Emin, The sign of the Hall effect in hopping conduction, Philos. Mag. **35**, 1189 (1977).

[9] W. C. Germs, W. H. Adriaans, A. K. Tripathi, W. S. C. Roelofs, B. Cobb, R. A. J. Janssen, G. H. Gelinck, and M. Kemerink, Charge transport in amorphous InGaZnO thin-film transistors, Phys. Rev. B **86**, 155319 (2012).

[10] T. Kamiya, K. Nomura, and H. Hosono, Electronic structures above mobility edges in crystalline and amorphous In-Ga-Zn-O: percolation conduction examined by analytical model, J. Display Technol. **5**, 462 (2009).

[11] D. Adler, L. P. Flora, and S. D. Senturia, Electrical conductivity in disordered systems, Solid State Commun. **12**, 9 (1973).

[12] T. Kamiya, K. Nomura, and H. Hosono, Origin of definite Hall voltage and positive slope in mobility-donor density relation in

disordered oxide semiconductors, Appl. Phys. Lett. **96**, 122103 (2010).

[13] S. Lee, K. Ghaffarzadeh, A. Nathan, J. Robertson, S. Jeon, C. Kim, I.-H. Song, and U.-I. Chung, Trap-limited and percolation conduction mechanisms in amorphous oxide semiconductor thin film transistors, Appl. Phys. Lett. **98**, 203508 (2011).

[14] K. Abe, N. Kaji, H. Kumomi, K. Nomura, T. Kamiya, M. Hirano, and H. Hosono, Simple analytical model of on operation of amorphous In-Ga-Zn-O thin-film transistors, IEEE Trans. Electron Devices **58**, 3463 (2011).

[15] K. Abe, K. Takahashi, A. Sato, H. Kumomi, K. Nomura, T. Kamiya, and H. Hosono, Operation model with carrier-density dependent mobility for amorphous In–Ga–Zn–O thin-film transistors, Thin Solid Films **520**, 3791 (2012).

[16] K. Abe, A. Sato, K. Takahashi, H. Kumomi, T. Kamiya, and H. Hosono, Mobility- and temperature-dependent device model for amorphous In–Ga–Zn–O thin-film transistors, Thin Solid Films **559**, 40 (2014).

[17] F. J. Blatt, *Physics of Electronic Conduction in Solids* (McGraw-Hill Book Company, New York, 1968).

[18] See Supplemental Material at http://link.aps.org/supplemental/10.1103/PhysRevB.95.045208 for details on sample preparation, measurement methods and device modeling.

[19] D. Long and J. Myers, Ionized-impurity scattering mobility of electrons in silicon, Phys. Rev. **115**, 1107 (1959).

[20] P. Lawaetz, Low-field mobility and galvanomagnetic properties of holes in germanium with phonon scattering, Phys. Rev. **174**, 867 (1968).

[21] Y.-H. Kim, M.-K. Han, J.-I. Han, and S. K. Park, Effect of metallic composition on electrical properties of solution-processed indium-gallium-zinc-oxide thin-film transistors, IEEE Trans. Electron Dev. **57**, 1009 (2010).

[22] S. Jeong, Y.-G. Ha, J. Moon, A. Facchetti, and T. J. Marks, Role of gallium doping in dramatically lowering amorphous-oxide processing temperatures for solution-derived indium zinc oxide thin-film transistors, Adv. Mater. **22**, 1346 (2010).